



## Highly active nanostructured palladium-ceria electrocatalysts for the hydrogen oxidation reaction in alkaline medium

Hamish R Miller, Francesco R Vizza, Marcello R Marelli, Anicet R Zadick, Laetitia R Dubau, Marian R Chatenet, Simon Geiger, Serhiy R Cherevko, Huong A Doan, Ryan R Pavlicek, et al.

### ► To cite this version:

Hamish R Miller, Francesco R Vizza, Marcello R Marelli, Anicet R Zadick, Laetitia R Dubau, et al.. Highly active nanostructured palladium-ceria electrocatalysts for the hydrogen oxidation reaction in alkaline medium. *Nano Energy*, 2017, 33, pp.293 - 305. <10.1016/j.nanoen.2017.01.051>. <hal-01533467>

**HAL Id: hal-01533467**

**<https://hal.science/hal-01533467v1>**

Submitted on 15 Oct 2018

**HAL** is a multi-disciplinary open access archive for the deposit and dissemination of scientific research documents, whether they are published or not. The documents may come from teaching and research institutions in France or abroad, or from public or private research centers.

L'archive ouverte pluridisciplinaire **HAL**, est destinée au dépôt et à la diffusion de documents scientifiques de niveau recherche, publiés ou non, émanant des établissements d'enseignement et de recherche français ou étrangers, des laboratoires publics ou privés.



HAL Authorization

# Highly active nanostructured palladium-ceria electrocatalysts for the hydrogen oxidation reaction in alkaline medium<sup>†</sup>

Hamish A. Miller<sup>a\*</sup>, Francesco Vizza<sup>a\*</sup>, Marcello Marelli<sup>b</sup>, Anicet Zadick<sup>c,d</sup>, Laetitia Dubau<sup>c,d</sup>, Marian Chatenet<sup>c,d,e</sup>, Simon Geiger<sup>f</sup>, Serhiy Cherevko<sup>f,g</sup>, Huong Doan<sup>h</sup>, Ryan K. Pavlicek<sup>h</sup>, Sanjeev Mukerjee<sup>h</sup>, and Dario R. Dekel<sup>i,j,\*</sup>

<sup>a</sup> Istituto di Chimica dei Composti Organometallici (CNR-ICCOM), via Madonna del Piano 10, 50019 Sesto Fiorentino, Firenze, Italy.

<sup>b</sup> Istituto di Scienze e Tecnologie Molecolari (ISTM-CNR) via Camillo Golgi 19, 20133 Milano, Italy.

<sup>c</sup> University of Grenoble Alpes, LEPMI, F-38000 Grenoble, France

<sup>d</sup> CNRS, LEPMI, F-38000 Grenoble, France

<sup>e</sup> French University Institute (IUF), Paris, France

<sup>f</sup> Department of Interface Chemistry and Surface Engineering, Max-Planck-Institut für Eisenforschung GmbH, 40237 Düsseldorf, Germany

<sup>g</sup> Helmholtz-Institute Erlangen-Nürnberg for Renewable Energy (IEK-11), Forschungszentrum Jülich, 91058 Erlangen, Germany

<sup>h</sup> Department of Chemistry and Chemical Biology, Northeastern University, Boston, MA, 02115, USA

<sup>i</sup> The Wolfson Department of Chemical Engineering, Technion – Israel Institute of Technology, Haifa, 3200003, Israel.

<sup>j</sup> The Nancy & Stephan Grand Technion Energy Program (GTEP), Technion – Israel Institute of Technology, Haifa 3200003, Israel.

<sup>†</sup>Electronic Supplementary Information (ESI) available: [Experimental details and Figs.]. See DOI: 10.1039/b000000x/

**Abstract:**

We report an interesting new class of bifunctional electrocatalysts, Pd/C-CeO<sub>2</sub>, with excellent activity and stability for the hydrogen oxidation reaction (HOR) under alkaline conditions. The unique structure of palladium deposited onto a mixed support of Vulcan XC-72 carbon and CeO<sub>2</sub> consists of Pd metal preferably deposited on the ceria regions of the catalyst. The CeO<sub>2</sub>-Pd interaction leads to enhanced HOR kinetics and increased stability. Here we compare catalysts with three different Pd loadings and show that the 10 wt% Pd sample has optimized activity. Hydrogen pumping and fuel cell experiments based on this catalyst show higher activities as compared to a Pd/C sample without ceria. Metal dissolution tests and identical location transmission microscopy experiments show that the catalyst stability under harsh potential cycling experiments in alkaline medium is significantly improved as compared to Pd/C, making this material one of the best options for use as highly active and highly stable electrocatalysts for the HOR in anion exchange membrane fuel cells.

## 1. Introduction:

Anion exchange membrane fuel cells (AEM-FCs) have received increasing attention as this technology has the potential to replace expensive platinum and platinum alloy materials currently used in fuel cell electrodes, significantly reducing the cost of fuel cell devices.[1] Recently, significant progress has been made in improving material components for AEM-FCs in particular cell hardware, membranes, ionomers and cathode catalysts for the oxygen reduction reaction (ORR).[2-13] However, the sluggish hydrogen oxidation reaction (HOR) kinetics of electrocatalysts under alkaline conditions have limited the development of affordable Pt-free catalysts and AEM-FC technology is still awaiting new advanced catalytic materials to fulfill its potential.[14] Hence, the realization of a completely Pt-free AEM-FC requires the development of novel anode catalyst structures that enhance the HOR of the supported metal nanoparticles (NPs).[15] A new class of Pd based materials that exploit mixed carbon and metal oxide supports has recently been reported that have led for the first time, to performances of non-Pt AEM-FCs with power densities around  $0.5 \text{ W cm}^{-2}$ , operating with partially filtered air at the cathode and dry hydrogen at the anode.[16] In particular, the addition of  $\text{CeO}_2$  to Vulcan XC-72 carbon with a 50:50 weight ratio yields a conductive support onto which Pd deposits preferentially onto the ceria regions (confirmed by EDX-STEM and XAS investigations).[16] When compared to a Pd supported on carbon catalyst (without ceria) with the same particle size distribution and metal loading, a 5-fold improvement is obtained in the anode performance under the same fuel cell conditions for the Pd/C- $\text{CeO}_2$  catalyst. It is believed that the presence of an intimate contact between ceria and Pd enhances the  $\text{OH}^-$  transfer from the anion conducting membrane and ionomer regions of the fuel cell to the metal surface where the HOR takes place.[17] Cyclic voltammetry (CV) studies have shown a weakening of the Pd-H bonding when ceria is in contact with Pd.[16] The oxidative desorption of hydrogen from Pd (Eqn. 1) is considered to be the rate determining step (rds) of the HOR under alkaline conditions (Eqn. 1).[18, 19]



Hence, a weakening of the bonding of the adsorbed hydrogen can enhance significantly the kinetics. Due to the increasing complexity and challenge of the mechanism of HOR in alkaline media as compared to HOR in acidic medium, the stability of the catalyst is of concern. Due to the scarce data available on HOR catalysts in alkaline medium, stability tests of these materials have not been reported. Specifically for Pd based catalysts, while Pd dissolution in acidic media is well

documented,[20, 21] literature data on Pd corrosion in alkaline media is very scarce. Also Pourbaix diagrams, showing stability windows for different species in the E vs. pH space, do not give any conclusive answer to whether Pd corrodes in base. According to a previous report, Pd should be extremely stable in typically used alkaline electrolytes.[22] In that report, the authors could not detect any signs of Pd dissolution in 0.5M KOH at 25°C. However, at alkali concentrations of 6M KOH or higher, and at elevated temperatures some dissolution was detected. Bolzan, interpreting the results obtained using rotating ring disk electrode tests, suggested that some Pd dissolution exists in 1M NaOH, but stressed that the dissolution rates/amounts are significantly lower than that measured in acidic electrolytes.[23] More recently, however, using identical-location transmission electron microscopy (ILTEM) coupled to electrochemistry, Zadick *et al.* demonstrated that the relative stability of Pd towards electrochemical dissolution in base was not a warranty for the stability of state-of-the-art carbon supported Pd nanoparticles at high pH. Indeed, the particles suffer dramatic detachment from their carbon support, overall yielding a very large decrease of electrochemical surface area (ECSA) in a rather limited number of voltammetric cycles (typically below 1000 cycles at 100 mV s<sup>-1</sup> in the range 0.1 < E < 1.23 V vs RHE) in 0.1 M NaOH at 25°C.[24] Surprisingly, Pt/C nanoparticles were demonstrated to suffer even more such degradation in base electrolytes.[25]

In the present study, we report our continued investigation of the properties of the Pd/C-CeO<sub>2</sub> catalyst, showing its enhanced HOR activity in a hydrogen-pumping cell, confirming the ceria effect on the catalytic activity of the Pd. We also report further details on its properties by comparing different Pd ratios on the same C-CeO<sub>2</sub> support (6wt%, 10wt% and 20wt% Pd). Finally, several stability studies of the Pd-C-CeO<sub>2</sub> catalyst are also reported here for the first time, using both *in situ* inductively coupled plasma mass spectrometry (ICP-MS) and identical-location transmission electron microscopy experiments, as well as using hydrogen-pumping cells.

## 2. Experimental

All material manipulations during materials preparation, except as stated otherwise, were routinely performed under nitrogen atmosphere using standard airless technique. Carbon black (Vulcan XC-72 pellets) was purchased from Cabot Corp., USA. All metal salts and reagents were purchased from Aldrich and used as received. All the solutions were freshly prepared with doubly distilled deionized water.

## 2.1. Material syntheses

### 2.1.1. Synthesis of Pd/C (10 wt%):

Vulcan XC-72 (6.0 g) was suspended in 250 ml of ethylene glycol and sonicated for 20 min in a 500 ml three-neck round-bottomed flask. Then a solution of 1.0 g of  $\text{PdCl}_2$  in a mixture of  $\text{H}_2\text{O}$  (50 mL), ethylene glycol (50 mL) and 6 mL HCl (37%) was added dropwise under stirring in a  $\text{N}_2$  stream. After adequate stirring, an alkaline solution of NaOH (5g) in  $\text{H}_2\text{O}$  (10 mL) and ethylene glycol (35 mL) was introduced in the reactor which then was heated at 125 °C for 3 h again under a  $\text{N}_2$  atmosphere. Then the mixture was cooled to room temperature. The solid product was filtered off and washed with  $\text{H}_2\text{O}$  to neutral pH. The final product was dried in vacuum oven at 40 °C. (Yield: 6.53 g).

### 2.1.2. Synthesis of C-CeO<sub>2</sub> support (50:50):

Vulcan XC-72 (4g) was added to a solution of  $\text{Ce}(\text{NO}_3)_3 \cdot 6\text{H}_2\text{O}$  (10.1g) in  $\text{H}_2\text{O}$  (250 mL). The mixture was kept under stirring for 60 min and sonicated for 30 min. After adjusting the pH to 12 with KOH, the resulting suspension was stirred for 2 hours. The product was separated by filtration and washed with  $\text{H}_2\text{O}$  until neutral pH was obtained. The product was dried at 65°C, then subsequently heated under air in a tube furnace at 250°C for 2 hours. Cooling to room temperature was undertaken under a flow of Ar. The yield of C-CeO<sub>2</sub> was 7.15g.

### 2.1.3. Synthesis of Pd/C-CeO<sub>2</sub>:

The synthetic procedure used was the same for each catalyst with the only difference the amount of Pd salt used to obtain the desired loading of 6wt%Pd, 10wt%Pd and 20wt%Pd. As an example for the 10wt%Pd catalyst, the synthesis was as follows: C-CeO<sub>2</sub> (4g) was suspended in water (500mL), stirred vigorously for 30 min and sonicated for 20 min. To this mixture, a solution of  $\text{K}_2\text{PdCl}_4$  (1.38g) in water (60mL) was slowly added (during ca. 1 hour) under vigorous stirring, followed by addition of an aqueous solution of 2.5M KOH (8.4mL). Next, ethanol (50mL) was added and the resulting mixture was heated at 80°C for 60 min. The desired product Pd/C-CeO<sub>2</sub> was filtered off, washed several times with distilled water to neutrality and finally dried under vacuum at 65°C until constant weight was reached. The yield of Pd/C-CeO<sub>2</sub> was 4.45g.

## 2.2 Electrochemical and physical characterization

Transmission electron microscopy (TEM) was performed on a Philips CM12 microscope at an accelerating voltage of 100kV. The microscope was equipped with an EDAX energy dispersive microanalysis system. Scanning Electron Microscopy (SEM) was performed on a HITACHI S4800 microscope operating at 15kV. High resolution TEM (HR-TEM) images were recorded with a Zeiss Libra 200 FE TEM equipped with a double tilt goniometer at 200kV and FEI Tecnai-F30 microscope which was operated at 300kV. The active metal surface area was determined by CO chemisorption method, adapted to carbon supported materials, at 70°C by the use of an ASAP 2020C Instrument (Micromeritics Corp.). Before the measurements, the samples were reduced at 210°C with H<sub>2</sub> and treated in vacuum at the same temperature for 15 hours.

Cyclic Voltammetry (CV) measurements were performed with a Princeton 2273A potentiostat/galvanostat, using a three-electrode arrangement with an Ag/AgCl reference electrode and a platinum foil (25mm x 25mm x 0.1mm) as counter electrode. No IR drop compensation was applied to any of the performed experiments. The potential scale of the CV curves was then converted to the reversible hydrogen electrode (RHE) scale.

Procedures for cell preparation for fuel cell tests are described elsewhere.[16] Membrane electrode assemblies (MEAs) (5cm<sup>2</sup> active area) consisting of Ag alloy-based cathodes and Pd/C-CeO<sub>2</sub> based anodes with 6wt%Pd, 10wt%Pd, and 20wt%Pd that were activated by operating at 50mV in clean air (~10ppm CO<sub>2</sub>) (1sLPM, 1barg, dew point 73°C) and dry hydrogen (0.2sLPM, 3barg, room temperature), while heating the cell from room temperature to 73°C. Following temperature and current density stabilization, polarization curves were measured from 50mV to open-circuit at a constant scanning rate of 0.1 V min<sup>-1</sup>.

Hydrogen pump experiments were carried out using 5cm<sup>2</sup> electrodes. For the purposes of these tests, three different materials were evaluated as Hydrogen Oxidation Reaction (HOR) catalysts. Commercial Pt/C (46wt%, 3mg<sub>Pt</sub>/cm<sup>2</sup> + 20% ionomer layer) was used as a standard, while 10wt% Pd/C (0.33mg<sub>Pd</sub>/cm<sup>2</sup> + 27% ionomer layer) and 10wt%Pd/C-CeO<sub>2</sub> (0.38mg<sub>Pd</sub>/cm<sup>2</sup> + 30% ionomer layer) were also evaluated. In all cases, Pt/C electrodes identical to the standard were used as CE/RE electrodes for the Hydrogen Evolution Reaction (HER). Electrodes were prepared by spraying an ink solution composed of water, IPA, catalyst, and Nafion onto bare carbon paper supports. An additional topcoat of ionomer was also sprayed onto the electrodes. Prior to use, anion exchange membranes were hydrated for 2 hours in 65°C water, followed by a room temperature solution of 0.5M NaOH

for 1 hour to complete the exchange process. The MEAs was hot-pressed for 4 minutes under a 3600lb load (100psi) at 60°C.

Testing was done on in-house built test stations, with a cell operating temperature of 60°C with 100% relative humidity. During cell heating and humidification, N<sub>2</sub> was flowed over both electrodes at 100sccm. Anode flow was then switched to H<sub>2</sub> at 100sccm, while the cathode flow remained unchanged.

Stabilization of the MEA was achieved by slowly ramping from 10 to 100mA cm<sup>-2</sup> (10mA cm<sup>-2</sup> increments, 1 minute per step), followed by a 30 minute hold at 100mA cm<sup>-2</sup>. Polarization curves were taken from 50 to at least 300 mA cm<sup>-2</sup> in 50 mA cm<sup>-2</sup> increments, followed by a 1 hour hold at 300 mA cm<sup>-2</sup>. All measurements were taken on a Metrohm Autolab (PGSTAT302N) paired with a 20A current booster (PGSTAT30). Electrochemical Impedance Spectra (EIS) were taken potentiostatically at the potentials corresponding to the polarization curve current densities.

A modified scanning flow cell (SFC) with a 2mm in diameter opening connected to an inductively coupled plasma mass spectrometer (ICP-MS, NexION, 300X, Perkin Elmer) was used to perform a first set of electrochemical stability tests.[26] The Pd<sup>106</sup> signal was recorded in relation to the Rh<sup>103</sup> as an internal standard, which was added downstream of the SFC. The flowrate was 180 μL min<sup>-1</sup>. All measurements were done in a 0.05M NaOH electrolyte. A glassy carbon plate was employed as the working electrode to support Pd/C-CeO<sub>2</sub> (10wt%Pd) and Pd/C (10wt%Pd) catalysts, while a graphite rod and an Ag/AgCl electrode were used as the counter and reference electrodes, respectively. All potentials are reported against the RHE. For preparation of the catalyst ink 8.5mg of Pd/C-CeO<sub>2</sub> or Pd/C was suspended in 5mL ultrapure water with addition of 20μL Nafion-solution (5wt%, Sigma-Aldrich). After ultrasonic treatment 0.3μL of the suspension were drop-casted on the glassy carbon plate, which after drying, led to the formation of circular spots of ca. 1mm in diameter. The resulting catalyst loading was of 6.5 μg<sub>Pd</sub> cm<sup>-2</sup>. Afterwards, the carbon plate containing catalyst spots was fixed under the SFC. The catalyst spots were located with the help of a vertical camera attached to the SFC. During measurements the SFC was always placed in such a way that the geometrical centre of the cell and catalyst spot coincided.

Additional stability tests were performed by applying a sequence of CVs in supporting electrolyte at room temperature. The stability procedures used in this study are essentially similar to those used in the literature [24, 25] to monitor the degradation of Pd/C nanoparticles (deposited on the same Vulcan XC72 carbon substrate than here and with a similar loading in Pd. A catalyst ink was prepared by mixing 10mg of Pd/C-CeO<sub>2</sub> catalyst powder, 6.74mL of ultrapure water (18.2MΩ cm, < 3ppb TOC,



Elix + Milli-Q Gradient, Millipore), 18.8  $\mu\text{L}$  of Nafion® solution (5wt% in water and light alcohols, Electrochem. Inc.®) and 33.9  $\mu\text{L}$  of isopropanol. From this ink, 20  $\mu\text{L}$  was deposited at a 5 mm-diameter glassy carbon tip, yielding a surface Pd loading of *ca.* 13  $\mu\text{g}_{\text{Pd}} \text{ cm}^{-2}$ .

The electrochemical experiments were performed in a classical three-electrode cell connected to a VSP numeric potentiostat (Bio-Logic®). The electrolyte was an Ar-purged aqueous solution of 0.1M NaOH at room temperature ( $T=25^\circ\text{C}$ ); this supporting electrolyte was prepared using high-purity reagents (Merck, Suprapur®) and ultrapure water. The counter-electrode was a carbon plate to avoid pollution issues by metal cations. Hg/HgO was used as reference electrode in the same electrolyte, the potential of which was verified by comparison with a freshly-prepared RHE. All the potential values are nevertheless expressed on the RHE scale. The accelerated stress tests (AST) consisted of 150 and then 1000 CV cycles in the supporting electrolyte, within a potential range of  $0.1 < E < 1.23$  V vs. RHE; the potential sweep rate was 100  $\text{mV s}^{-1}$ . During this AST, CV cycles were periodically monitored. The morphology of the Pd/C-CeO<sub>2</sub> nanoparticles was also characterized by identical-location transmission electron microscopy (ILTEM) after 150 and 1000 CV cycles. In that case, the above-mentioned AST was reproduced using a gold + lacey carbon TEM grids as the working electrode. In ILTEM, similar regions of the catalyst are observed before/after the degradation test. The TEM used for these specific characterizations is a JEOL 2010 TEM apparatus, equipped with a LaB6 filament operating at 200 kV (point to point resolution 0.19 Å) and with an Oxford Inca® X-Ray dispersive spectrometer for local chemical analyses.

### 3. Results and Discussion:

#### 3.1 Material characterization

The XRD diffraction patterns of the as prepared catalyst materials are shown in Figure 1. Trace 1(a) represents the mixed carbon-ceria support and all visible peaks can be assigned to ceria-based reflections. The addition of Pd to the support can be seen by the appearance of a peak at around  $40^\circ$  that can be assigned to Pd metal. The small intensity and broad nature of the peak for these samples is representative of the presence of a large proportion of amorphous Pd oxides in each catalyst as has been confirmed by XAS studies in our previous report.[16] This is particularly obvious when comparing the intensity with that representative of the Pd/C sample (10wt% Pd) in trace (e) where most of the Pd present is metallic. In-situ XRD studies have shown that the Pd oxide in the C-CeO<sub>2</sub> supported samples is reduced metal in the presence of flowing hydrogen.[16]

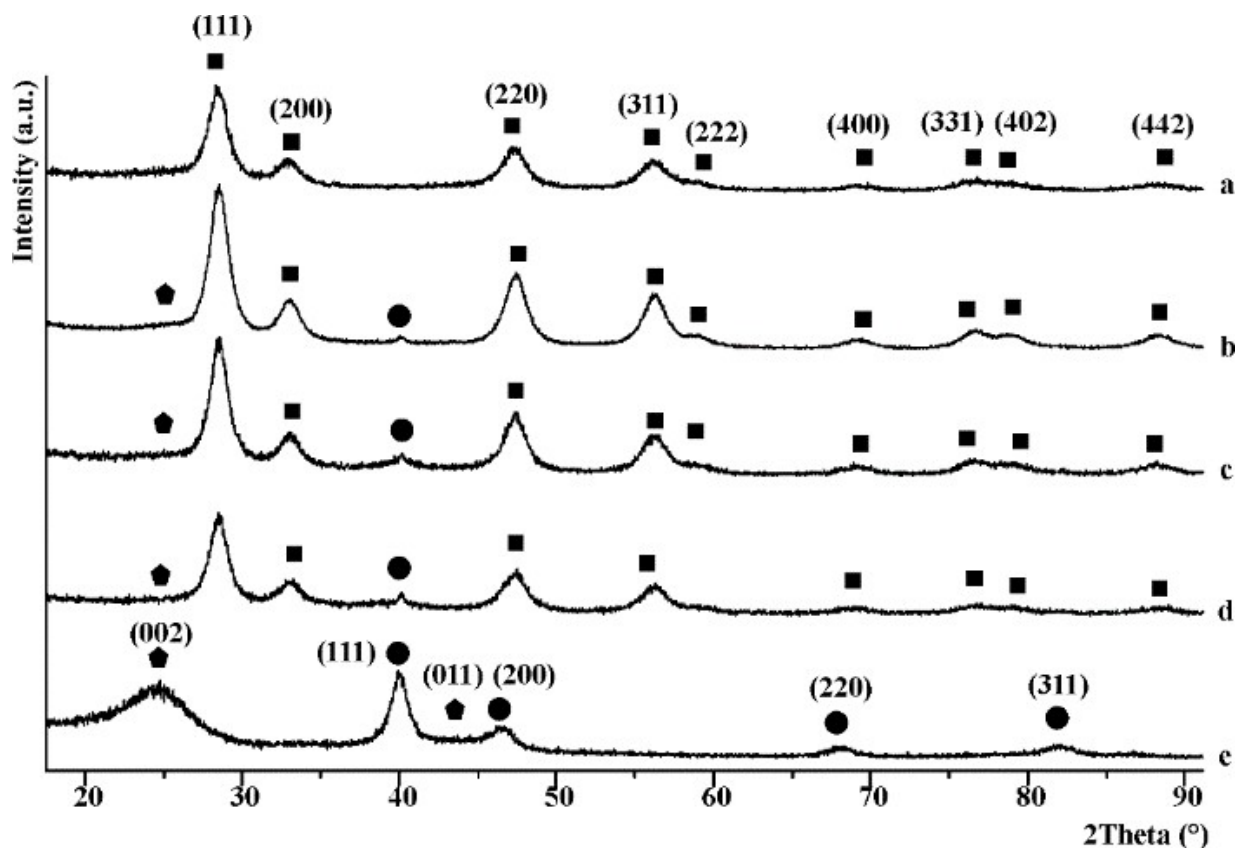


Figure 1. XRD diffraction patterns of (a) 50:50wt% C-CeO<sub>2</sub>, (b) Pd/C-CeO<sub>2</sub> (6wt% Pd), (c) Pd/C-CeO<sub>2</sub> (10wt% Pd), (d) Pd/C-CeO<sub>2</sub> (20wt% Pd) and (e) Pd/C (10wt% Pd). Legend: (●) Pd, (■) CeO<sub>2</sub> and (◆) carbon.

The specific surface area ( $S_{\text{BET}}$  m<sup>2</sup> g<sup>-1</sup>) of these materials was determined using Brunauer–Emmett–Teller (BET) analysis (Table 1). The value obtained for the as-obtained Vulcan XC-72R (222 m<sup>2</sup> g<sup>-1</sup>) is in the range of what reported in the literature.[27] The addition of ceria which has a BET surface area of approximately 60 m<sup>2</sup> g<sup>-1</sup> [28] to Vulcan XC-72 carbon with a 50:50 weight ratio reduces the surface area of the resulting mixed support C-CeO<sub>2</sub> (140 m<sup>2</sup> g<sup>-1</sup>). Addition of 6 or 10wt% Pd to C-CeO<sub>2</sub> does not affect significantly the values of specific surface area measured. With 20 wt% Pd, the BET surface area drops from around 140 to 124 m<sup>2</sup> g<sup>-1</sup>. Table 1 also shows the active metal (Pd) surface area determined by CO chemisorption experiments. The data reported includes the Pd specific surface area m<sup>2</sup> g<sup>-1</sup><sub>Pd</sub> and the average crystallite size calculated from this data (nm). The 10wt% Pd sample shows the highest Pd specific surface area (236 m<sup>2</sup> g<sub>Pd</sub><sup>-1</sup>) and smallest calculated crystallite size (2.1 nm).

Table 1: Physical characterization data obtained from BET experiments and CO-chemisorption isotherms.

| Sample                                       | $S_{\text{BET}}$<br>$\text{m}^2 \text{g}^{-1}$ | Pd specific<br>surface area<br>$\text{m}^2 \text{g}^{-1}_{\text{Pd}}$ | Pd particle size<br>nm |
|--|--|---|------------------------|
| C (Vulcan XC-72)                             | 222  | -   | -                      |
| C-CeO <sub>2</sub> (50wt% CeO <sub>2</sub> ) | 140  | -   | -                      |
| Pd/C-CeO <sub>2</sub> (6wt% Pd)              | 141  | 188   | 2.6                    |
| Pd/C-CeO <sub>2</sub> (10wt% Pd)             | 145  | 236   | 2.1                    |
| Pd/C-CeO <sub>2</sub> (20wt% Pd)             | 124  | 146   | 3.4                    |

To study the catalyst morphology and surface structure, we have found that high resolution Z-contrast STEM is a good technique to elucidate the structure of these catalysts and the Pd metal distribution. In Figure 2, images at different magnifications are shown for the Pd/C-CeO<sub>2</sub> materials with different Pd loadings (6 wt%, 10 wt% and 20 wt% of Pd). Firstly, it can be seen that the CeO<sub>2</sub> particles do not cover uniformly the Vulcan XC-72 carbon material. Some distinct agglomerated CeO<sub>2</sub> structures (brighter structures) can be seen separated from the Vulcan carbon. Pd nanoparticles (NPs) are visible on the bare carbon areas. It is not possible however to individualize Pd NPs on the ceria portions due to poor resolution between these two species. The number of Pd NPs visible on the carbon substrate increases along with the loading. Interestingly, few Pd particles are visible on the 6wt% Pd sample (pointed out by arrows). More are visible on the carbon as the metal loading increases and this allows us to determine the average Pd particle size distribution (mean values determined are 2.0nm and 2.5nm for the 10wt% and 20wt% samples, respectively).

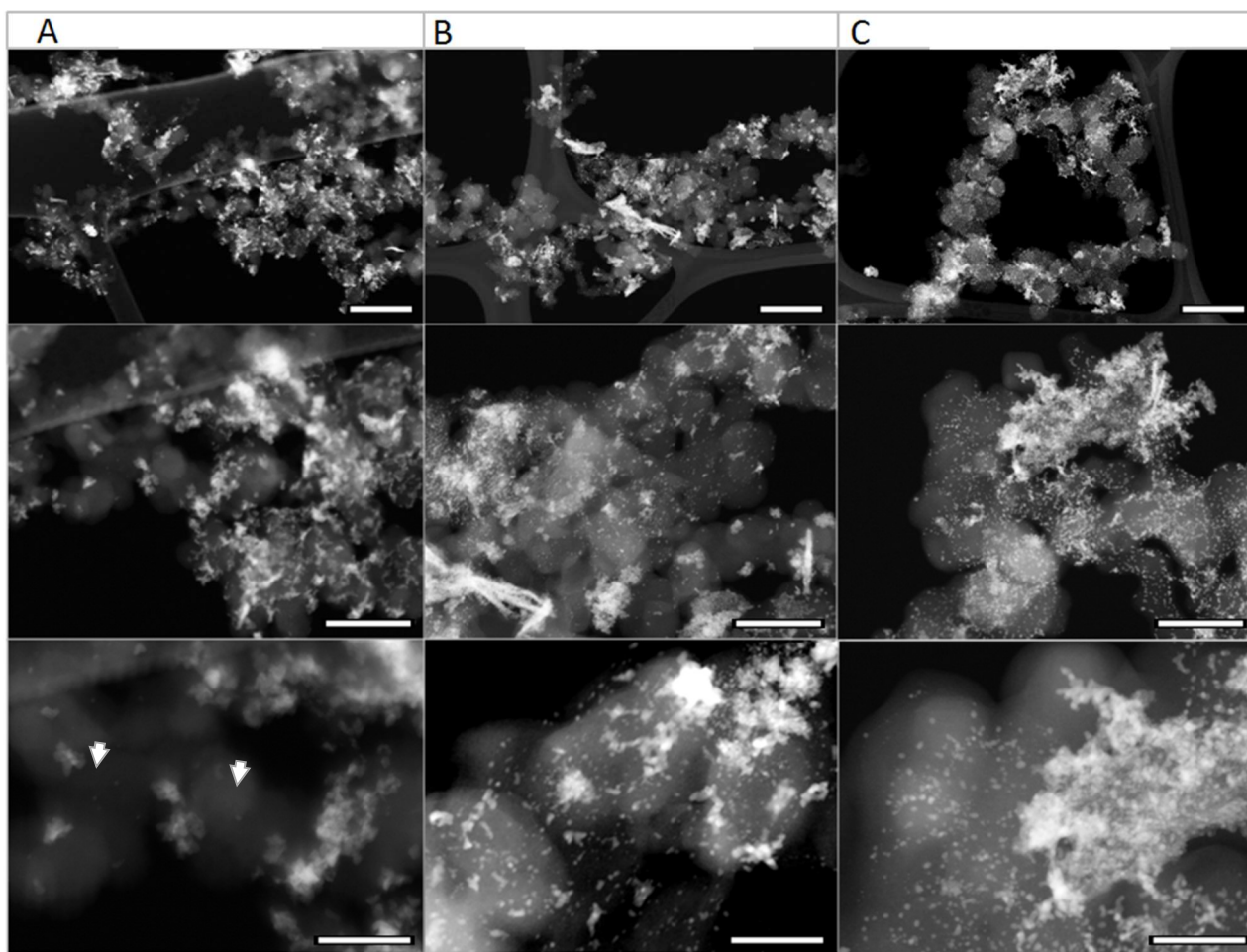


Figure 2: Comparison between the three Pd loadings (A 6%, B 10% and C 20 %) at three different magnifications: scale bar of the first line is 200nm, middle line 100nm and bottom line 50nm.

STEM-EDX analysis helps to determine the Pd distribution over the whole sample including also the ceria portions of the support. As example, a representative image of the 20wt% Pd sample is shown in Figure 3. Two zones are clearly distinguishable. On the right side a purely carbon portion (in blue) covered with many small Pd NPs (in green). STEM-EDX elemental map analysis shows a large ceria cluster (in red) covering the carbon structure on the left portion of the sample. The Pd mapping shows that although there are many Pd NPs visible on the carbon section, most of the Pd is actually present on the ceria structures. STEM-EDX analysis of the sample prepared with 10 wt% Pd shows the same trend with the only difference being that very few Pd nanoparticles are visible on the bare carbon regions (see SI for comparative analysis). The middle set of TEM images in Figure 2 also show clearly that there are few Pd nanoparticles visible on the carbon regions for 6 and 10 wt% Pd samples while at 20 % loading there is higher coverage of Pd also on the carbon.

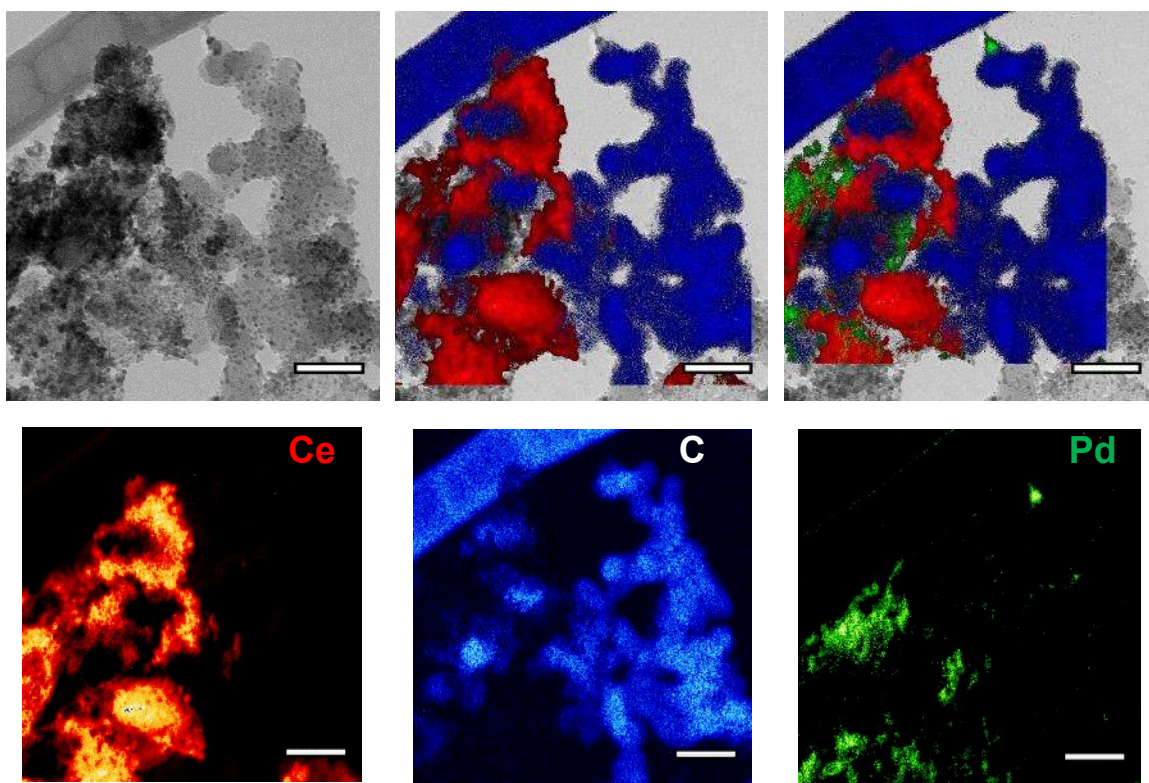


Figure 3: STEM-EDX analysis of a representative portion of the 20wt% Pd catalyst (scale bar 50 nm).

### 3.2 Electrochemical tests

Electrochemical data are listed in Table 2, including the electrochemically active surface area (ECSA), exchange current densities ( $i^0$ ) and the mass activity per gram of Pd ( $i^0$ , m). The mass activity per gram of Pd is significantly higher for the 10 wt% Pd sample relative to both the 6 wt% and 20 wt% samples. The Tafel analysis of each catalyst, shown in Figure 4, also confirms the increased performance of the 10wt% Pd sample relative to the others. Indeed, increasing the Pd loading from 10% to 20% does not improve the overall activity of the catalyst. Tafel slope analysis reveals a large difference amongst the various catalysts with values of 100, 66 and 143 mV dec<sup>-1</sup> respectively suggesting a change in the HOR mechanism after a doubling of the Pd loading (10 to 20%). A value of 66 mVdec<sup>-1</sup> indicates that the rate determining step (rds) for the 10% Pd catalyst is molecular hydrogen dissociative adsorption (Tafel step), while the 20% Pd sample shows a value that suggests charge transfer processes are rate limiting.[19]

Table 2: Electrochemical characterization data.

| Pd content<br>in Pd/C-CeO <sub>2</sub><br>wt% | $i_0$<br>$\mu\text{A cm}_{\text{Pd}}^{-2}$ | ECSA<br>$\text{m}^2 \text{g}_{\text{Pd}}^{-1}$ | Tafel slope<br>$\text{mV dec}^{-1}$ | $i_{0, \text{m}}$<br>$\text{A g}_{\text{Pd}}^{-2}$ |
|---|--|--|-------------------------------------|--|
| 6   | 89   | 22   | 100                                 | 19   |
| 10  | 55   | 43   | 66                                  | 24   |
| 20  | 83   | 14   | 143                                 | 11   |

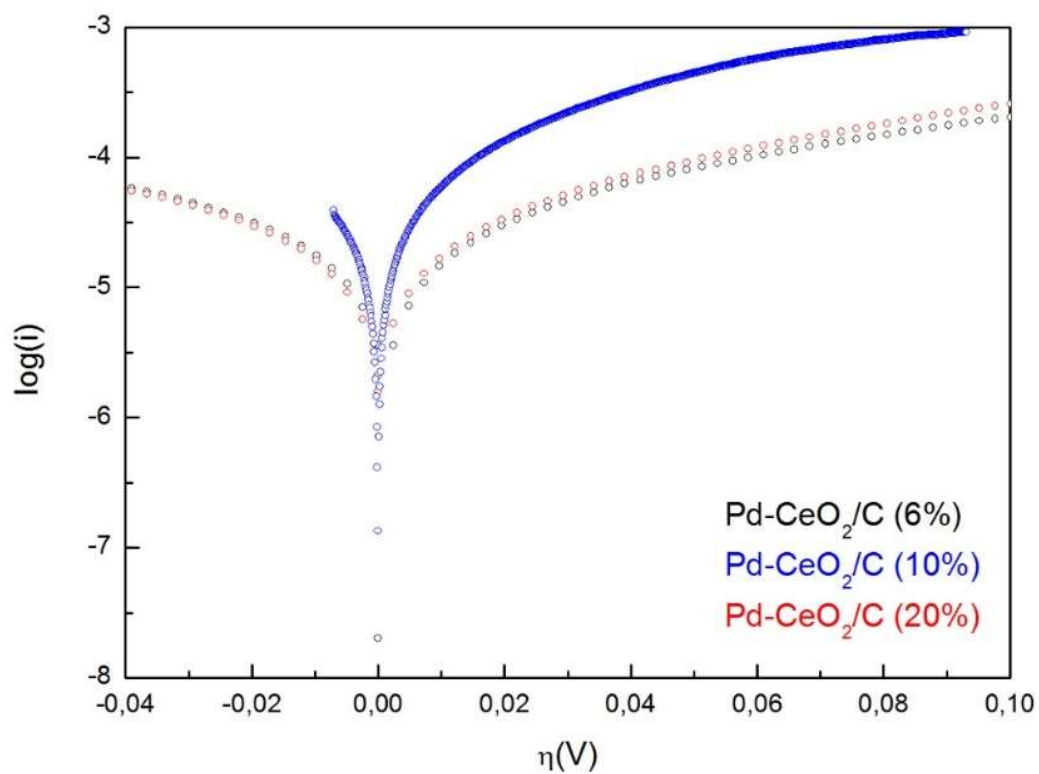


Figure 4. Tafel slope analysis of Pd/C-CeO<sub>2</sub> (6wt%, 10wt% and 20wt% Pd) obtained in H<sub>2</sub>-saturated 0.1M KOH at 10mV s<sup>-1</sup> and 1600rpm.



### 3.3 Fuel cell tests

For fuel cell tests, the Pd/C-CeO<sub>2</sub> anode catalysts with different Pd loadings (6wt%, 10wt% and 20wt% Pd) were incorporated into anode catalyst layers (0.15-0.30 mg<sub>Pd</sub> cm<sup>-2</sup>). Three identical cells where the only change was the anode catalyst layer, were prepared for testing in AEM-FC single cells. Figure 5 shows the cell performance at 73 °C run with dry H<sub>2</sub> and purified air (~10ppm CO<sub>2</sub>). Polarization curves of cells with anodes made with Pd/C-CeO<sub>2</sub> (6 and 20wt% Pd) were compared with the previous reported results made with anodes made with Pd/C-CeO<sub>2</sub> 10wt% Pd.[16] As can be seen from Figure 5, although results obtained with all catalysts appear to be similar, the Pd/C-CeO<sub>2</sub> 10wt% Pd reported previously shows slightly better performance.[16] Table 3 summarizes the fuel cell results.

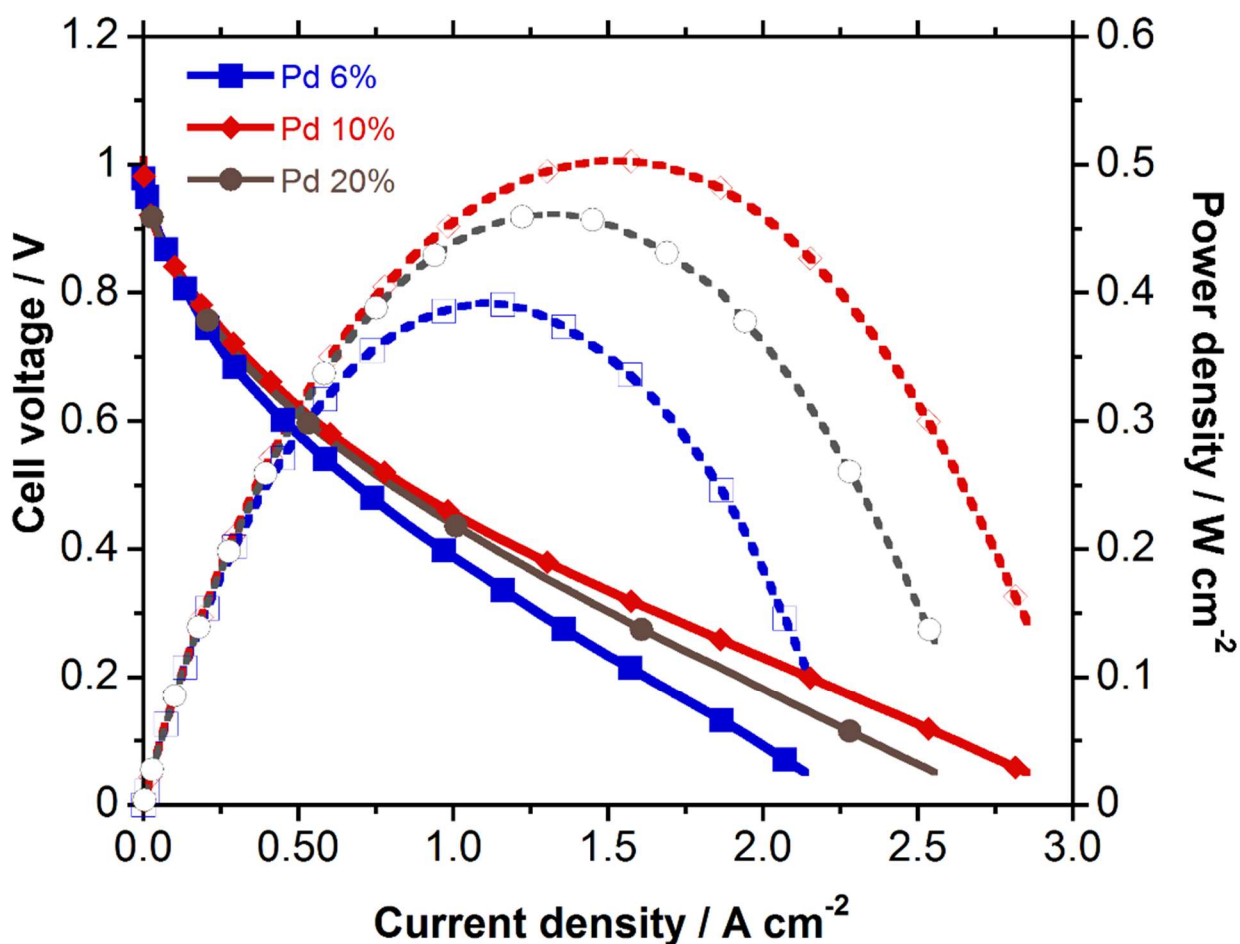


Figure 5. Polarization curves of AEM-FCs using Pd/C-CeO<sub>2</sub> anode catalysts with 10wt% Pd,[16] 6%Pd and 20wt%.

Table 3: H<sub>2</sub>/air AEM-FC polarization data summary

|                                      | Current density at 0.85V<br>mA cm <sup>-2</sup> | Peak power density<br>mW cm <sup>-2</sup> |
|--------------------------------------|---|---|
| Pd/C-CeO <sub>2</sub> 10wt%Pd [[16]] | 100   | 500                                       |
| Pd/C-CeO <sub>2</sub> 6wt%Pd         | 90  | 390                                       |
| Pd/C-CeO <sub>2</sub> 20wt%Pd        | 80  | 460                                       |

As shown in Table 3, the performance of the Pd/C-CeO<sub>2</sub> 10wt% Pd catalyst performs slightly better than the other two catalysts with higher and lower Pd loadings. It seems that the high Pd loading (20wt%) does not give any beneficial effect on fuel cell performance, as increasing the amount of Pd from 10wt% to 20wt% leads to more Pd deposited on the carbon regions, as discussed previously and also shown in Figures 2 and 3. These isolated Pd on carbon nanoparticles do not contribute to the enhanced activity as they perform as Pd/C, with significantly lower performance due to the lack of the advantage of Pd-ceria interactions.[16]

### 3.4 Hydrogen pumping tests

A hydrogen pump cell system was developed to test the best performing catalyst Pd/C-CeO<sub>2</sub> (10 wt%) and compare it to Pd/C (10 wt%) and Pt/C (46 wt%). This system allows us to study the HOR activity of each catalyst under fuel cell type conditions. Figure 6 shows the polarization curves for the three materials, demonstrating that the Pd/C-CeO<sub>2</sub> material far outperforms the Pd/C catalyst, while showing similar performance to that of a Pt/C anode. This is achieved with a Pd metal loading ~10 times lower than the Pt metal loading (0.33mg<sub>Pd</sub> cm<sup>-2</sup> vs. 3mg<sub>Pt</sub> cm<sup>-2</sup>).



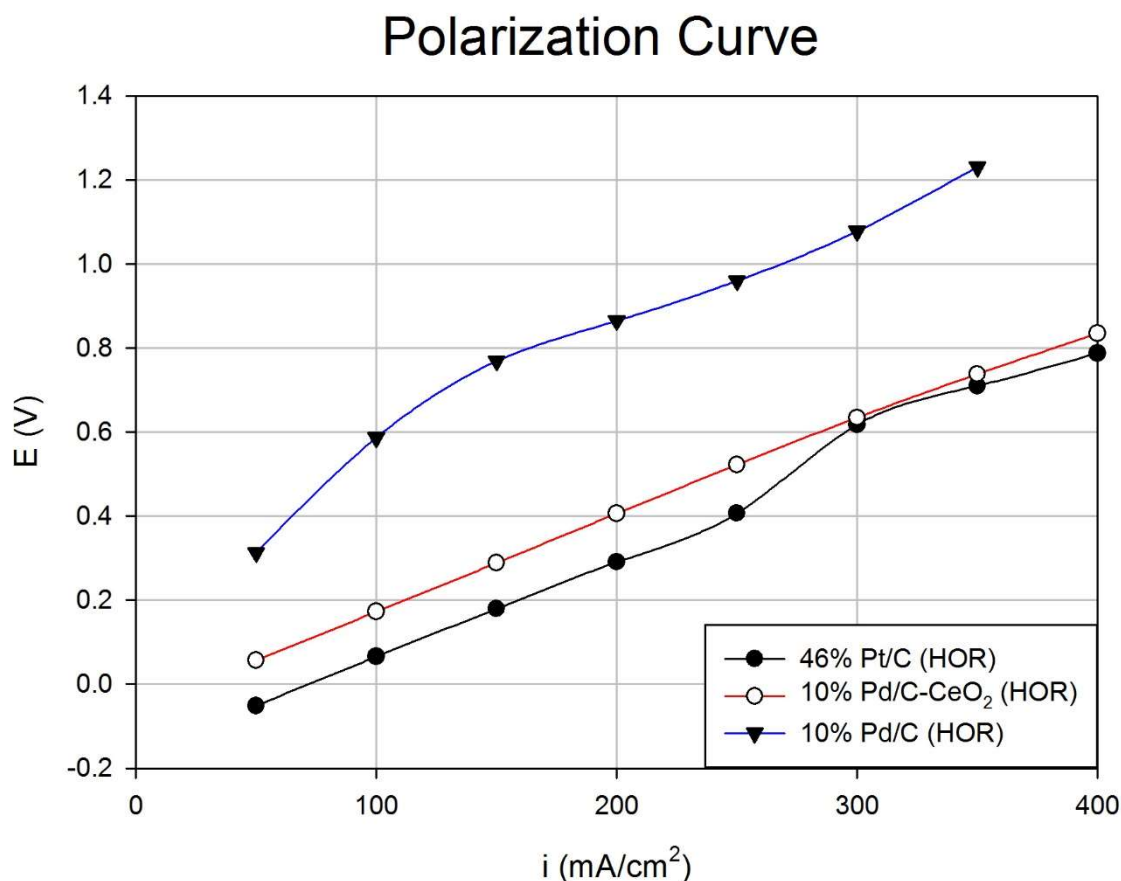


Figure 6. Polarization curves of hydrogen pumping tests comparing the HOR performance of Pd/C-CeO<sub>2</sub> to both Pd/C as well as Pt/C.

As can be seen, the performance of the Pd/C-CeO<sub>2</sub> catalyst is clearly superior to that obtained with Pd/C. For instance, at 0.4V and 0.8V the current densities obtained with Pd/C-CeO<sub>2</sub> were around three times higher than the current densities obtained with Pd/C. These results confirm the higher activity of Pd/C-CeO<sub>2</sub> as compared to Pd/C (without ceria) as has also been shown in fuel cell tests.[16]

Figure 7 shows the steady state performance of a hydrogen pumping cell run at constant 300 mA cm<sup>-2</sup> over the course of 1 hour. While the Pd/C shows an increase in potential during test, Pd/C-CeO<sub>2</sub> (as well as Pt/C) shows a very stable performance at a much lower potential. These results indicate that the addition of ceria support to the catalyst improves not just the performance, but also the stability of the catalyst.

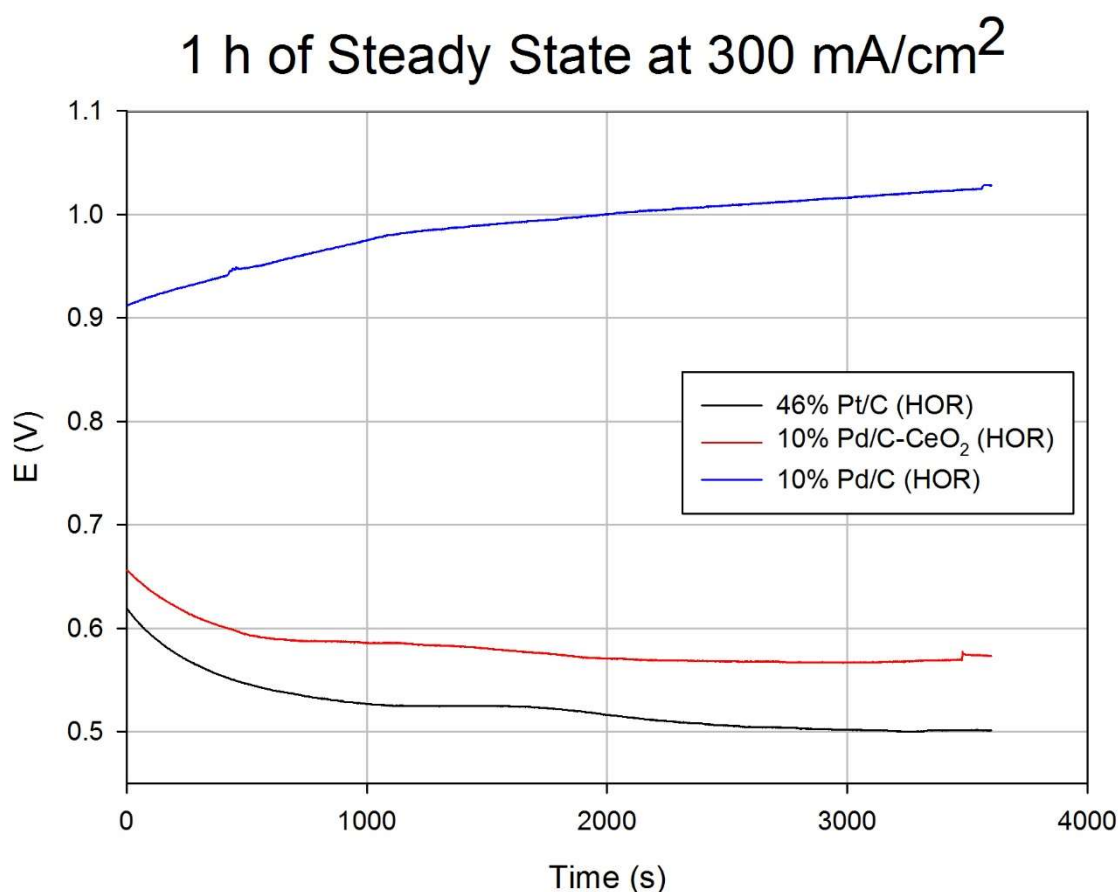


Figure 7. Stability run of hydrogen pumping tests of Pd/C-CeO<sub>2</sub> catalyst as compared to both Pd/C and Pt/C under 300mA cm<sup>-2</sup> steady state operation.

Electrochemical Impedance Spectroscopy (EIS) spectra were taken for all three HOR catalysts. Figure 8 summarizes these results for  $J = 300\text{mA cm}^{-2}$ . All three materials showed negative shifts in the high-frequency resistance (HFR) as the current density increased. The shift in the Pt/C HFR was significantly larger ( $\sim 25\text{m}\Omega$ ) than either the Pd/C ( $\sim 5\text{m}\Omega$ ) or the Pd/C-CeO<sub>2</sub> ( $\sim 15\text{m}\Omega$ ). The charge transfer resistance (approximated by the distance between the two y-intercepts) of the Pt/C was less than that of either of the two Pd-based materials. However, the Pd/C-CeO<sub>2</sub> did show an improvement over the Pd/C catalyst. Additionally, the HFR of the Pd/C-CeO<sub>2</sub> catalyst was very similar to that of the Pt/C reference.

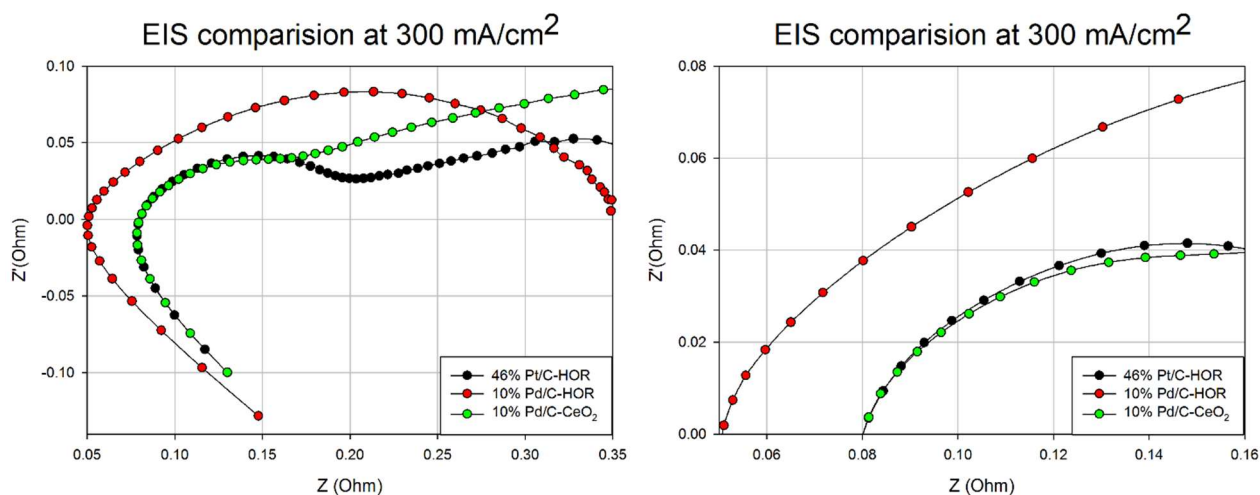


Figure 8. EIS measured during hydrogen pumping tests at a current density of  $300 \text{ mA cm}^{-2}$ . Right plot shows a zoom-in of the left plot.

### 3.5 Stability tests

To further evaluate the stability of Pd/C-CeO<sub>2</sub>, electrochemical tests were performed using a modified SFC to measure the dissolution properties of the 10wt% Pd/C-CeO<sub>2</sub> catalyst in alkaline medium compared to Pd/C. To get a first insight on the stability of the studied catalysts in alkaline media, CVs in a broad potential window ( $-0.05$  to  $1.4 \text{ V}_{\text{RHE}}$ ) of Pd oxide formation and reduction as well as hydrogen sorption and desorption were recorded in Ar-saturated  $0.05 \text{ M NaOH}$  electrolyte. The results are summarized in Figure 9.

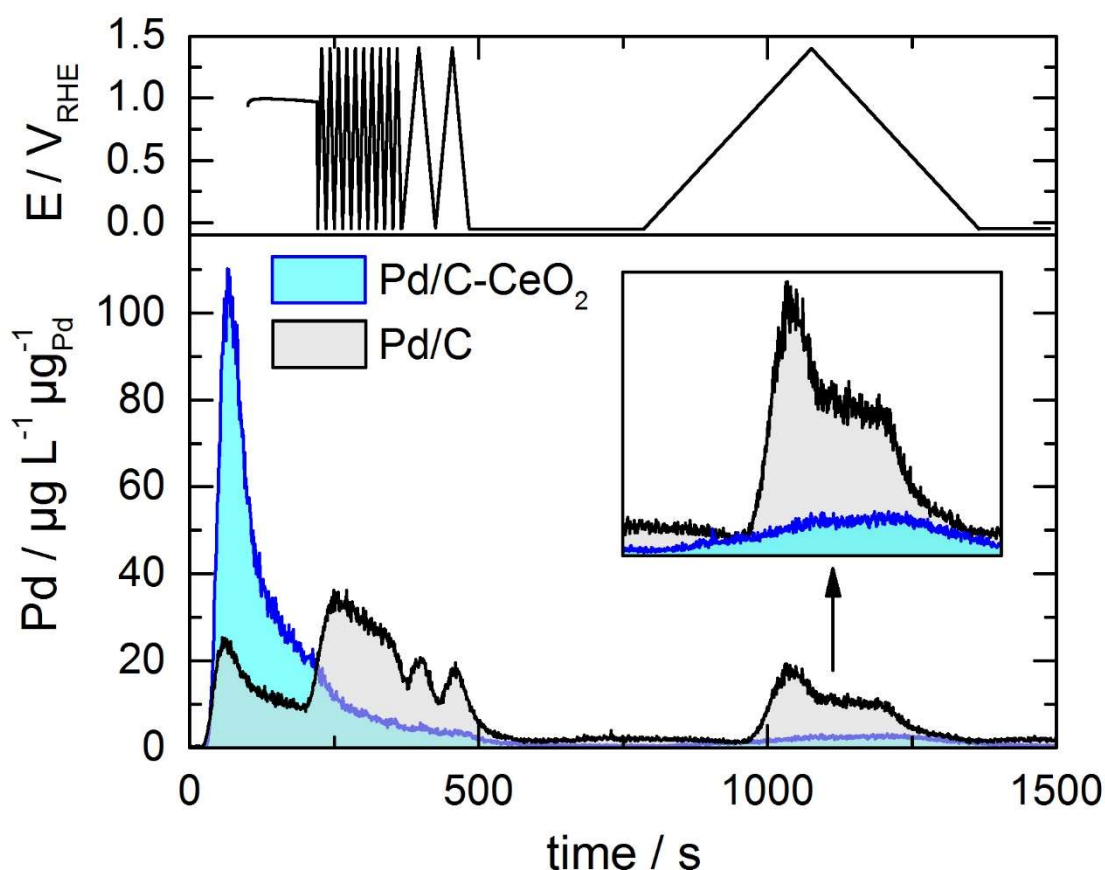


Figure 9. Pd detection profiles of Pd/C and Pd/C-CeO<sub>2</sub> (both 10wt% Pd) during 10 cycles at 200mVs<sup>-1</sup>, 2 cycles at 50mVs<sup>-1</sup> and 1 cycle at 5mVs<sup>-1</sup>, in the range of -0.05 to 1.4 V<sub>RHE</sub> in 0.05M NaOH purged with Argon.

In Figure 9 the upper pane shows variation of potential with time. This contains a short stay at the open circuit potential (OCV), fast cleaning cycles, two cycles recorded at 50mVs<sup>-1</sup>, short potentiostating at -0.05V<sub>RHE</sub>, and a slow scan at 5mV s<sup>-1</sup>. The latter is added for a clear separation between anodic and cathodic dissolution processes, well known for corrosion of other noble metals in acid and base.[29] Dissolution is shown in the lower pane in Figure 9. By comparing the Pd/C-CeO<sub>2</sub> catalyst with Pd/C one can clearly see that the OCV is slightly lower, while more Pd is detected in this region for Pd/C-CeO<sub>2</sub>. This can be an indication of the cathodic dissolution of an unstable Pd oxide, which is consistent with the fact that Pd oxide is found in the Pd/C-CeO<sub>2</sub> catalyst before flowing hydrogen, which reduces the oxide layer to Pd metal (see section 3.1). Since also some cerium dissolution was observed in this region (see Figure S2), it can be assumed that the two processes are related, as it was found that Pd was preferable deposited on ceria regions (see section 3.1). It has to

be remarked though, that the observed signal must be due to dissolution but not particle detachments as in the latter case the dissolution rates of Pd and Ce should scale linearly.

From Figure 9 it can be also seen that the Pd/C-CeO<sub>2</sub> catalyst stabilizes with potential cycling, although the detection of Pd by ICP-MS is still non-zero. The contrary is observed for Pd/C where Pd detection from this electrode significantly increases with potential cycling. The origin of the detection of Pd can here originate both from dissolution of the Pd nanoparticles or from their detachment from the carbon support, the latter having been found non-negligible in NaOH electrolytes by ILTEM experiments.[24] The total amount of Pd lost from both electrodes during the OCV and the potential cycling is ca. 1.4ng, which is 3% of the initial loading. Both electrodes are stabilized during the following potential step at  $-0.05\text{ V}_{\text{RHE}}$ . When potentials move into anodic direction, Pd starts to dissolve from both electrodes. Interestingly, the onset of Pd dissolution from Pd/C-CeO<sub>2</sub> is significantly lower than for Pd/C (see inset in Figure 9), suggesting a different mechanism (or different kinetics) of Pd loss. Even if initiated later, Pd/C dissolution however, shows much higher dissolution rates (up to an order of magnitude) at the higher potentials. At even higher potentials Pd passivates, likely due to formation of a stable oxide. Some increase in dissolution is also observed during oxide reduction, although the amounts are lower. As previously indicated, the reason for the superior stability of Pd/C-CeO<sub>2</sub> may be a strong Pd-ceria interaction. As demonstrated by STEM and XAS investigations in our recent article most of the Pd nanoparticles are supported on the CeO<sub>2</sub> (and not on carbon),[16] and are therefore not subjected to the harsh nanoparticle detachment that occurs for carbon-supported Pd/C nanoparticles. This hypothesis will be explored by ILTEM experiments (see below).

It is anticipated that during normal operation of an AEM-FC the highest anodic potential the anode will experience is the potential at open circuit (0.9V-1.0V vs RHE), which is significantly lower than the upper potential limit of cycling used in the experiments presented in Figure 9 (=1.4V vs RHE). Also, as hydrogen can influence (reduce) the Pd oxide layer of the Pd/C-CeO<sub>2</sub> catalyst, a second protocol shown in Figure 10 was used to investigate Pd stability at much more realistic conditions (better simulating an AEM-FC environment). In this case, the upper potential limit was moved to 1.0 V<sub>RHE</sub> and the cleaning cycles were excluded. Moreover, dissolution was studied in argon as well as in hydrogen, to test if hydrogen influences stability and to see if the improved activity of Pd/C-CeO<sub>2</sub> towards HOR holds also in SFC tests.

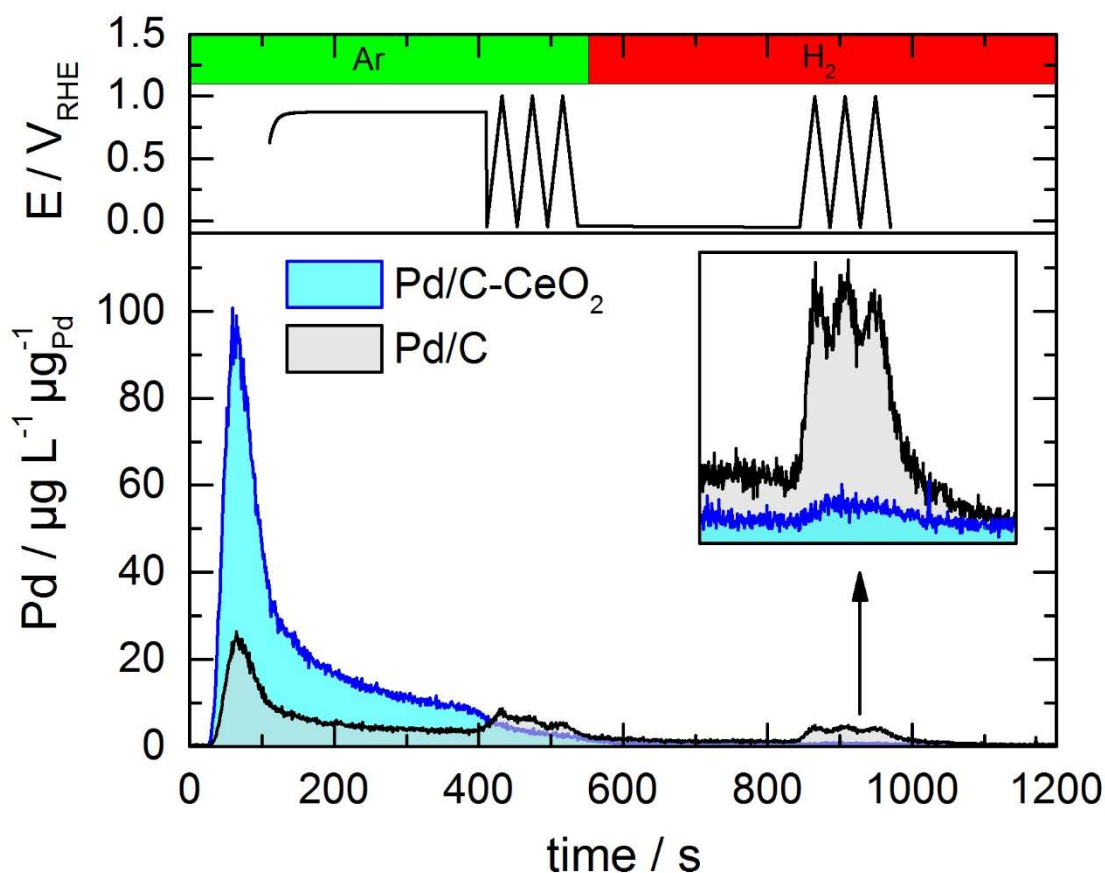


Figure 10. Dissolution profiles of Pd/C and Pd/C-CeO<sub>2</sub> (10wt%Pd) during cycling at 50mV s<sup>-1</sup> in the range of -0.05 to 1.0 V<sub>RHE</sub> in 0.05M NaOH purged with argon (in first, green left area) and then with hydrogen (in second, red right area).

For both electrodes, the dissolution behavior during the OCV and potential cycling in argon is analogous to that discussed above. Furthermore, no significant difference was observed when the gas was switched to hydrogen. In hydrogen, Pd behaves similarly to Pt in acid.[30] The inset in Figure 10 presents a magnified view of the dissolution profile, where it can be clearly seen that the amount of Pd dissolved from Pd/C-CeO<sub>2</sub> is significantly lower as compared to that dissolved from Pd/C, indicating that the stability of the Pd/C-CeO<sub>2</sub> is remarkable higher than the stability of Pd/C. In this region, the estimated amount of dissolved Pd was 50pg and 5pg for Pd/C and Pd/C-CeO<sub>2</sub>, respectively. Hence, assuming that dissolution rate is not changing with material consumption (a very rough estimation) all Pd should be completely dissolved in 3000 and 30000 cycles up to 1.0 V<sub>RHE</sub> from the Pd/C and Pd/C-CeO<sub>2</sub> electrodes, respectively. These results suggest that the excellent stability of the Pd/C-CeO<sub>2</sub> may be related to the Pd-ceria interaction.

To further examine the stability of the Pd/C-CeO<sub>2</sub> catalyst and investigate the mechanisms of degradation of these materials, CV cycling tests were also performed and analyzed. Figure 11 presents a sequence of CVs obtained on the Pd/C-CeO<sub>2</sub> (10wt%Pd) catalyst upon aging in 0.1 M NaOH (at 25°C) supporting electrolyte. It can be seen that the overall shape of the CV is very similar to that obtained on the same material in 0.1M KOH, previously reported,[16] although in that latter case, the peak related to Pd-oxides reduction was more pronounced, because the upper vertex potential was larger (1.3V vs. RHE instead of 1.4 V vs. RHE) and the scan rate value was lower. One also clearly sees that the signature of Pd-hydrides and Pd-oxides gradually level off upon cycling.

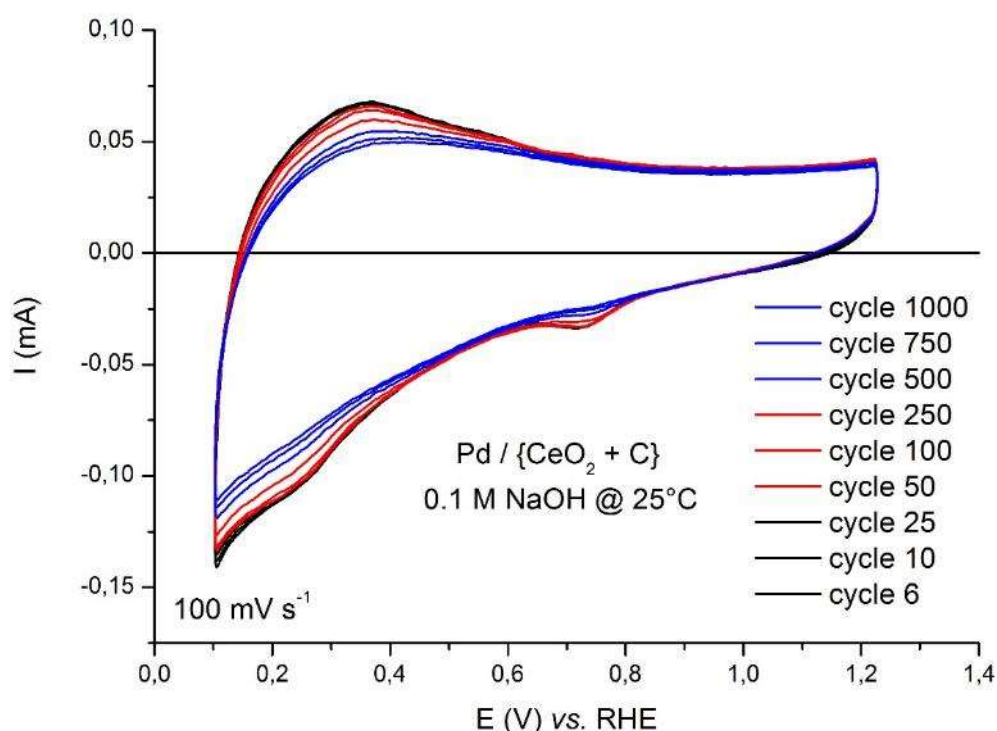


Figure 11. CVs monitored on the Pd/C-CeO<sub>2</sub> (10wt%Pd) catalyst upon aging in 0.1M NaOH supporting electrolyte at 25°C.

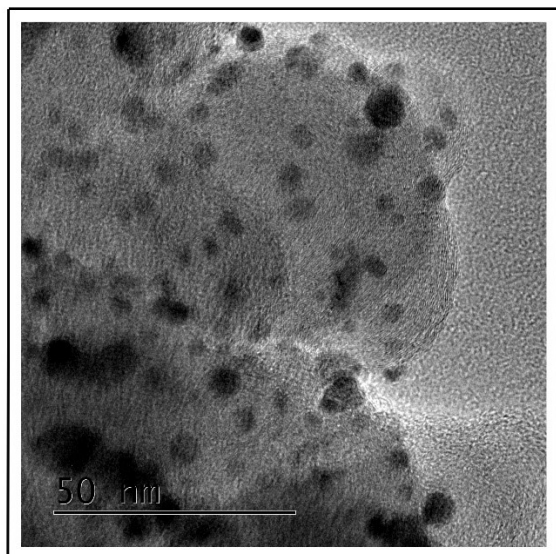
To complement the electrochemical experiments, ILTEM micrographs were acquired for Pd/C-CeO<sub>2</sub> after 150 and 1000 CV cycles (Figure 13) and for comparison, ILTEM micrographs of the Pd/C sample in its pristine state, and after 1000 CV are shown in Figure 12. For Pd/C (and this has been observed in a similar manner for “large” and “small” nanoparticles of Pd/C,[24, 25] more than 50% of the Pd nanoparticles were lost in the experiment, probably due to detachment of the nanoparticles

from the carbon substrate (Figure 12). Further stability tests are needed to clearly determine whether detachment of the particles actually occurs. Figure 13 shows for the same aging test with Pd/C-CeO<sub>2</sub>, that no major loss of Pd nanoparticles is observed, even after 1000 CV cycles.

In the case of the Pd/C-CeO<sub>2</sub> nanoparticles, the mechanisms at stake in the degradation test are completely different than for Pd/C. The micrographs of Figure 13 indeed show no consequent detachment of nanoparticles, but instead, their shape is progressively and severely modified upon cycling. Whereas the Pd crystallites of Pd/C-CeO<sub>2</sub> were (agglomerated but) small initially (*ca.* 2.1 nm in diameter,[24] they grow after 150 and especially 1000 CV cycles in supporting electrolyte. After 1000 CV, the originally agglomerated, small, and ill-defined Pd nanoparticles (all these observations agree with the results of XRD, CO-chemisorption and SEM/TEM presented above) are transformed into much larger and round-shape (for most of them) single crystalline nanoparticles (Figure 13). This process is a clear coalescence of the Pd nanoparticles initially present within agglomerates, probably according to a dissolution/redisposition mechanism on a short distance scale. It is worth noting that no new nanoparticles are created by the degradation, which rules out massive random redisposition, and the change of shape of isolated (not initially agglomerated) nanoparticles is very minimal, ruling out the *usual* 3D Ostwald ripening mechanism at long scale. In addition, it seems that when the Pd nanoparticles were initially not agglomerated (isolated), they remained isolated afterwards, and that the extent of detachment is much less than observed for a Pd/C sample (see Zadick et al.[25] and Figure 12). This is particularly obvious on the selected micrographs of Figure 14.



**Pristine**



**After 1000 CV cycles**

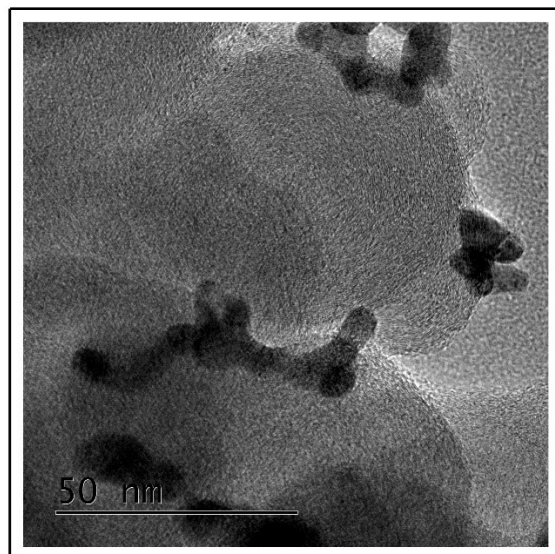


Figure 12. Selected ILTEM micrographs of the Pd/C sample in (A) its pristine state, and (B) after 1000 CV cycles in 0.1M NaOH at 25°C.

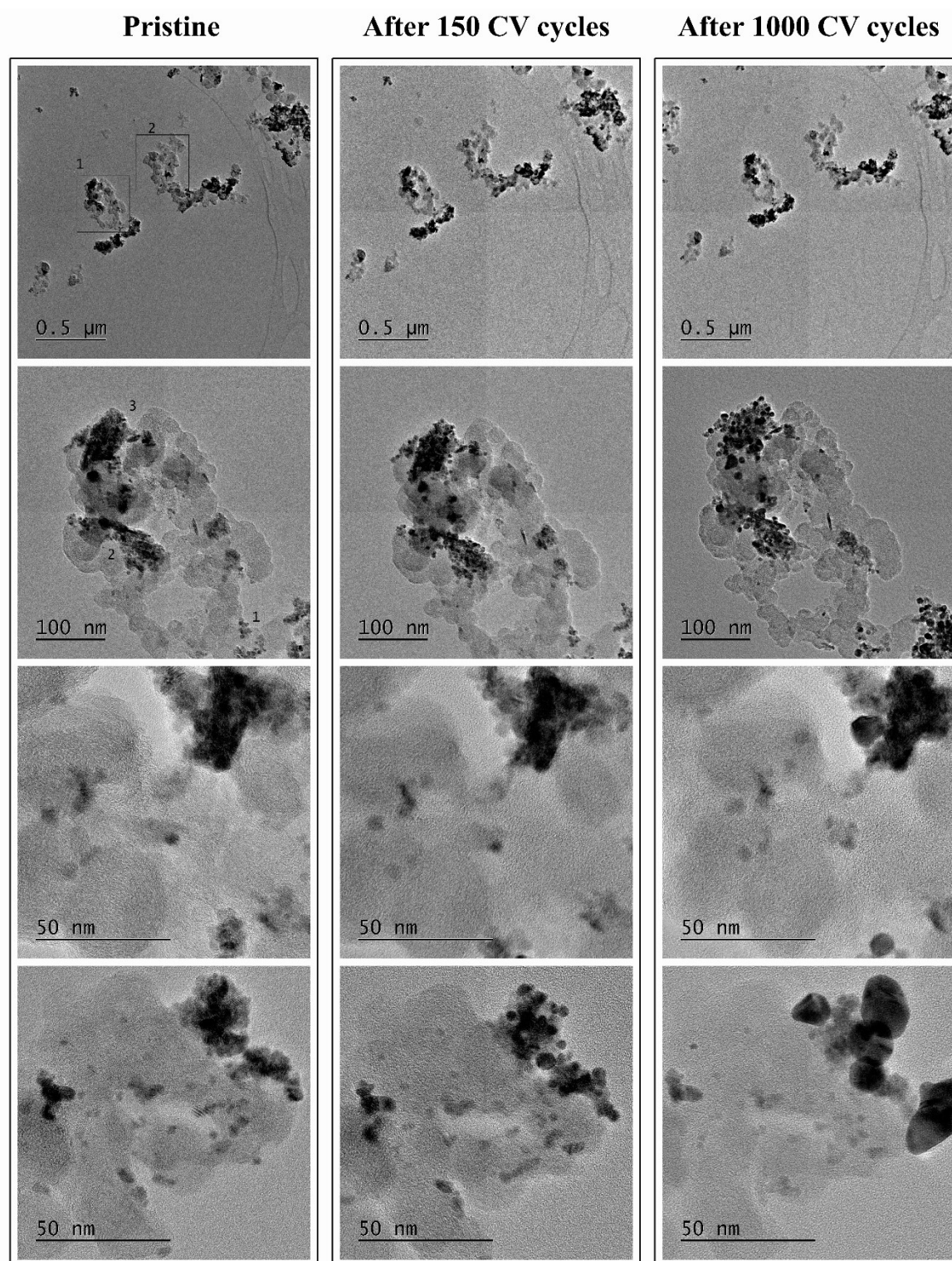


Figure 13 ILTEM micrographs of the Pd/C-CeO<sub>2</sub> sample in its pristine state (left), and after 150 (center) and then 1000 CV (right) cycles in 0.1M NaOH at 25°C. Although the vast majority of the Pd/C-CeO<sub>2</sub> nanoparticles undergo extensive agglomeration/coalescence (top micrographs), some (very few) regions are subjected to much less growth of the Pd crystallites and are subjected to (minor) loss of Pd nanoparticles (bottom micrographs).

In summary from ILTEM and CV aging studies, we can also say that the Pd/C-CeO<sub>2</sub> sample is much more stable in these operating conditions than its Pd/C counterpart. It is likely that the strong interaction of Pd with the CeO<sub>2</sub> and the related “more oxidized” state of Pd atoms do have a favorable impact on the durability of the Pd nanoparticles.[16] In addition, as most of the Pd nanoparticles in Pd/C-CeO<sub>2</sub> are in the vicinity of the CeO<sub>2</sub>, the latter being previously coated onto the Vulcan carbon, it can be speculated that the Pd nanoparticles in Pd/C-CeO<sub>2</sub> are mostly not in direct contact with the surface of the Vulcan carbon, as demonstrated in the high-resolution images of Figure 14. This hypothesis is also in agreement with the pronounced decrease of the BET area of the CeO<sub>2</sub>-coated Vulcan versus the pure Vulcan carbon (see section 3.1), which is compatible with the coating of the latter and related coverage/plugging of the micropores inside the carbon particles.

As it is precisely the interface of the Pd with carbon which is believed to be altered upon AST for the Pd/C samples (see Figure 12),[24] one may understand why the Pd/C-CeO<sub>2</sub> sample is more robust than Pd/C in terms of particle detachment. However, this robustness is not a guaranty of complete stability, since instead of particle detachment; the agglomerates of Pd nanoparticles supported on the C-CeO<sub>2</sub> substrate suffer extensive coalescence into larger nanoparticles. This extensive dissolution/redispersion essentially proceeds at short distance scale (essentially inside existing agglomerates but not from groups of nanoparticles separated by several 10nm or more), as illustrated in Figure 13. Figure 14 shows another remarkable example of such processes; in this case, the HRTEM images show that the grown Pd nanoparticle is clearly supported on CeO<sub>2</sub> crystals and not directly on the carbon substrate.

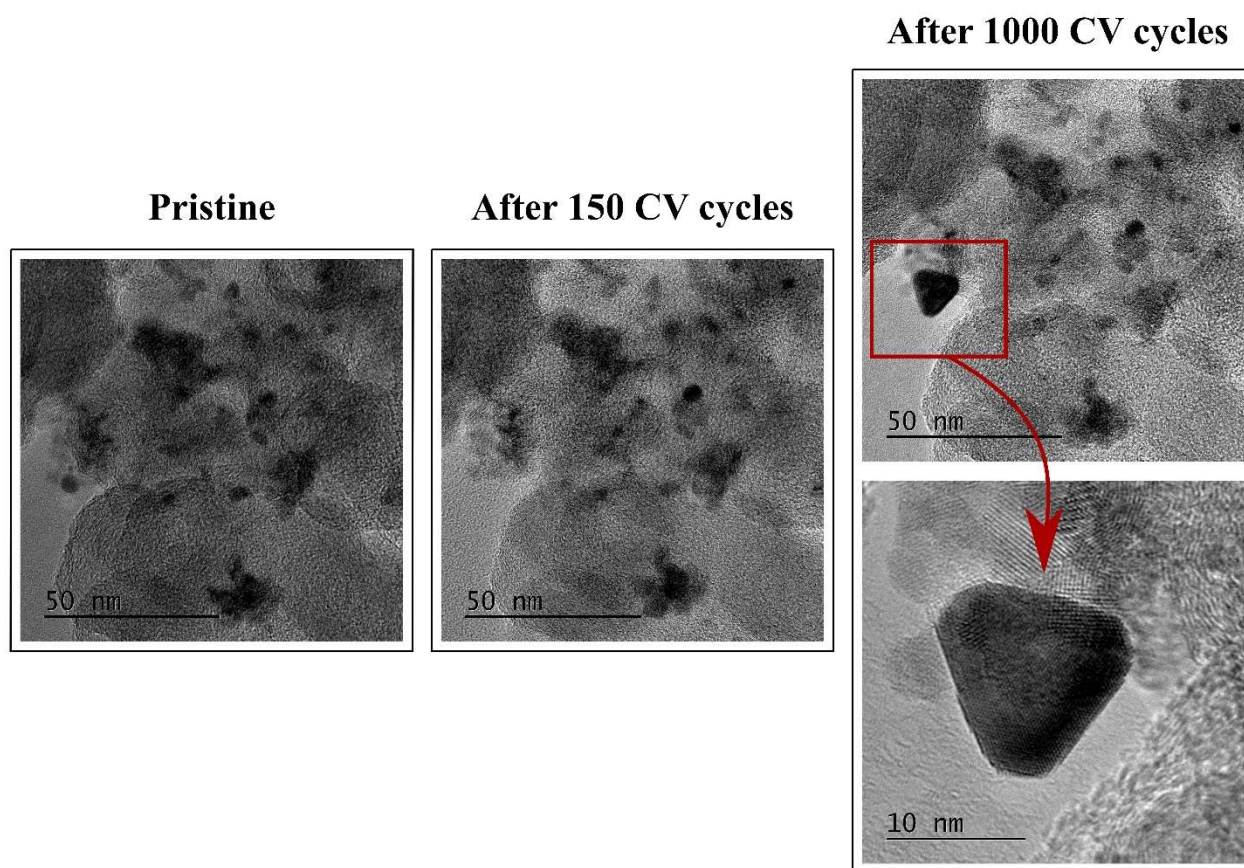


Figure 14. High-magnification micrographs of a grown monocrystalline Pd nanoparticle in contact with several smaller CeO<sub>2</sub> nanoparticles, for the Pd/C-CeO<sub>2</sub> catalyst; pristine (left), and after 1000 cycles (middle and right).

It can be pointed out that such dissolution/redispersion at short range agrees with the ICP-MS findings of Figures 9 and 10; such a process has also already been witnessed for unsupported Pd nanocubes.[31] Two hypotheses can be put forth to account for the different mechanisms of degradation of the Pd nanoparticles in Pd/C and Pd/C-CeO<sub>2</sub>: on the one hand, the fate of large Pd ensembles (agglomerates, more present in the initial Pd/C-CeO<sub>2</sub> sample than in the Pd/C ones previously[24] tested could differ from that of isolated Pd because (i) the proximity between individual crystallites in agglomerates could favor short-scale dissolution/redispersion of Pd or (ii) these large ensembles could have more anchoring points to the substrate. On the other hand, as previously hypothesized, it can be that the stability of the Pd/C-CeO<sub>2</sub> nanoparticles are uniquely linked to the proximity of Pd to the CeO<sub>2</sub> phase (anchoring points of the Pd nanoparticles to the Vulcan carbon (see Figure 12), which are prone to destruction in these conditions, are replaced by tougher anchoring points to the CeO<sub>2</sub> surface, see Figure 14), again in agreement with the findings of

ICP-MS. More studies are necessary to understand precisely the mechanisms of degradation of these materials, but this does not put into question the much enhanced durability of the Pd/C-CeO<sub>2</sub> nanoparticles noted here compared to Pd/C catalysts.

## **Conclusions**

We report a new class of bifunctional electrocatalyst for the hydrogen oxidation reaction in fuel cells under alkaline conditions. The electrocatalysts, denoted Pd/C-CeO<sub>2</sub>, consist of deposited Pd nanoparticles on a support mixture of 50:50 carbon and CeO<sub>2</sub>. The Pd is preferentially deposited on the ceria regions of the support. Previous reports on AEM-FCs as well as the hydrogen pump tests described in this report show that the Pd/C-CeO<sub>2</sub> catalyst has significantly higher activity than Pd/C towards the HOR in alkaline medium. In addition, we have performed preliminary stability studies on Pd/C-CeO<sub>2</sub> showing that catalyst stability under harsh potential cycling is improved as compared to Pd/C. To the best of our understanding, the Pd/C-CeO<sub>2</sub> bifunctional material studied in this report is the HOR electrocatalyst with highest activity and stability for AEM-FCs so far developed.

## **Acknowledgements**

We acknowledge the Ente Cassa di Risparmio di Firenze ITALY (projects HYDROLAB2 and EnergyLab) for financial support.

## References

- [1] J.R. Varcoe, P. Atanassov, D.R. Dekel, A.M. Herring, M.A. Hickner, P.A. Kohl, A.R. Kucernak, W.E. Mustain, K. Nijmeijer, K. Scott, T.W. Xu, L. Zhuang, Anion-exchange membranes in electrochemical energy systems, *Energ Environ Sci*, 7 (2014) 3135-3191.
- [2] Y.S. Li, T.S. Zhao, A passive anion-exchange membrane direct ethanol fuel cell stack and its applications, *Int J Hydrogen Energ*, 41 (2016) 20336-20342.
- [3] Y.S. Li, Y.L. He, An All-in-One Electrode for High-Performance Liquid-Feed Micro Polymer Electrolyte Membrane Fuel Cells, *J Electrochem Soc*, 163 (2016) F663-F667.
- [4] Y.S. Li, J.H. Lv, Y.L. He, A Monolithic Carbon Foam-Supported Pd-Based Catalyst towards Ethanol Electro-Oxidation in Alkaline Media, *J Electrochem Soc*, 163 (2016) F424-F427.
- [5] Y.S. Li, A liquid-electrolyte-free anion-exchange membrane direct formate-peroxide fuel cell, *Int J Hydrogen Energ*, 41 (2016) 3600-3604.
- [6] Y.S. Li, H. Wu, Y.L. He, Y. Liu, L. Jin, Performance of direct formate-peroxide fuel cells, *J Power Sources*, 287 (2015) 75-80.
- [7] Y.S. Li, Y.L. He, W.W. Yang, A high-performance direct formate-peroxide fuel cell with palladium-gold alloy coated foam electrodes, *J Power Sources*, 278 (2015) 569-573.
- [8] Y.S. Li, Y.L. He, Layer reduction method for fabricating Pd-coated Ni foams as high-performance ethanol electrode for anion-exchange membrane fuel cells, *Rsc Adv*, 4 (2014) 16879-16884.
- [9] J. Ponce-Gonzalez, D.K. Whelligan, L. Wang, R. Bance-Soualhi, Y. Wang, Y. Peng, H. Peng, D.C. Apperley, H.N. Sarode, T.P. Pandey, A.G. Divekar, S. Seifert, A.M. Herring, L. Zhuang, J.R. Varcoe, High performance aliphatic-heterocyclic benzyl-quaternary ammonium radiation-grafted anion-exchange membranes, *Energ Environ Sci*, 9 (2016) 3724-3735.
- [10] L. Wang, E. Magliocca, E.L. Cunningham, W.E. Mustain, S.D. Poynton, R. Escudero-Cid, M.M. Nasef, J. Ponce-Gonzalez, R. Bance-Souahli, R.C.T. Slade, D.K. Whelligan, J.R. Varcoe, An optimised synthesis of high performance radiation-grafted anion-exchange membranes, *Green Chem*, DOI 10.1039/c6gc02526a(2017).
- [11] E.F. Holby, P. Zelenay, Linking structure to function: The search for active sites in non-platinum group metal oxygen reduction reaction catalysts, *Nano Energy*, 29 (2016) 54-64.
- [12] O.V. Korchagin, V.A. Bogdanovskaya, M.R. Tarasevich, A.V. Kuzov, G.V. Zhutaeva, M.V. Radina, V.T. Novikov, V.V. Zharikov, Characteristics of Non-Platinum Cathode Catalysts for a Hydrogen-Oxygen Fuel Cell with Proton- and Anion-Conducting Electrolytes, *Catal Ind*, 8 (2016) 265-273.
- [13] K. Strickland, M.W. Elise, Q.Y. Jia, U. Tylus, N. Ramaswamy, W.T. Liang, M.T. Sougrati, F. Jaouen, S. Mukerjee, Highly active oxygen reduction non-platinum group metal electrocatalyst without direct metal-nitrogen coordination, *Nat Commun*, 6 (2015).
- [14] J. Durst, A. Siebel, C. Simon, F. Hasche, J. Herranz, H.A. Gasteiger, New insights into the electrochemical hydrogen oxidation and evolution reaction mechanism, *Energ Environ Sci*, 7 (2014) 2255-2260.
- [15] M. Alesker, M. Page, M. Shviro, Y. Paska, G. Gershinsky, D.R. Dekel, D. Zitoun, Palladium/nickel bifunctional electrocatalyst for hydrogen oxidation reaction in alkaline membrane fuel cell, *J Power Sources*, 304 (2016) 332-339.

- [16] H.A. Miller, A. Lavacchi, F. Vizza, M. Marelli, F. Di Benedetto, F.D.I. Acapito, Y. Paska, M. Page, D.R. Dekel, A Pd/C-CeO<sub>2</sub> Anode Catalyst for High-Performance Platinum-Free Anion Exchange Membrane Fuel Cells, *Angew Chem Int Edit*, 55 (2016) 6004-6007.
- [17] D. Strmcnik, M. Uchimura, C. Wang, R. Subbaraman, N. Danilovic, D. van der Vliet, A.P. Paulikas, V.R. Stamenkovic, N.M. Markovic, Improving the hydrogen oxidation reaction rate by promotion of hydroxyl adsorption, *Nat Chem*, 5 (2013) 300-306.
- [18] Y. Wang, G.W. Wang, G.W. Li, B. Huang, J. Pan, Q. Liu, J.J. Han, L. Xiao, J.T. Lu, L. Zhuang, Pt-Ru catalyzed hydrogen oxidation in alkaline media: oxophilic effect or electronic effect?, *Energ Environ Sci*, 8 (2015) 177-181.
- [19] S. St John, R.W. Atkinson, R.R. Unocic, T.A. Zawodzinski, A.B. Papandrew, Ruthenium-Alloy Electrocatalysts with Tunable Hydrogen Oxidation Kinetics in Alkaline Electrolyte, *J Phys Chem C*, 119 (2015) 13481-13487.
- [20] S. Cherevko, A.R. Zeradjanin, A.A. Topalov, N. Kulyk, I. Katsounaros, K.J.J. Mayrhofer, Dissolution of Noble Metals during Oxygen Evolution in Acidic Media, *Chemcatchem*, 6 (2014) 2219-2223.
- [21] B.R. Shrestha, A. Nishikata, T. Tsuru, Channel flow double electrode study on palladium dissolution during potential cycling in sulfuric acid solution, *Electrochim Acta*, 70 (2012) 42-49.
- [22] J.F. Llopis, Gamboa, J.M., and Victori L., *Electrochim Acta*, 17 (1972) 2225-2230.
- [23] A.E. Bolzan, Phenomenological Aspects Related to the Electrochemical-Behavior of Smooth Palladium Electrodes in Alkaline-Solutions, *J Electroanal Chem*, 380 (1995) 127-138.
- [24] A. Zadick, L. Dubau, U.B. Demirci, M. Chatenet, Effects of Pd Nanoparticle Size and Solution Reducer Strength on Pd/C Electrocatalyst Stability in Alkaline Electrolyte, *J Electrochem Soc*, 163 (2016) F781-F787.
- [25] A. Zadick, L. Dubau, N. Sergent, G. Berthome, M. Chatenet, Huge Instability of Pt/C Catalysts in Alkaline Medium, *Acs Catal*, 5 (2015) 4819-4824.
- [26] S.O. Klemm, A.A. Topalov, C.A. Laska, K.J.J. Mayrhofer, Coupling of a high throughput microelectrochemical cell with online multielemental trace analysis by ICP-MS, *Electrochem Commun*, 13 (2011) 1533-1535.
- [27] Y. Holade, C. Morais, K. Servat, T.W. Napporn, K.B. Kokoh, Enhancing the available specific surface area of carbon supports to boost the electroactivity of nanostructured Pt catalysts, *Phys Chem Chem Phys*, 16 (2014) 25609-25620.
- [28] N. Laosiripojana, S. Assabumrungrat, The effect of specific surface area on the activity of nano-scale ceria catalysts for methanol decomposition with and without steam at SOFC operating temperatures, *Chem Eng Sci*, 61 (2006) 2540-2549.
- [29] S. Cherevko, A.R. Zeradjanin, G.P. Keeley, K.J.J. Mayrhofer, A Comparative Study on Gold and Platinum Dissolution in Acidic and Alkaline Media, *J Electrochem Soc*, 161 (2014) H822-H830.
- [30] A.A. Topalov, A.R. Zeradjanin, S. Cherevko, K.J.J. Mayrhofer, The impact of dissolved reactive gases on platinum dissolution in acidic media, *Electrochem Commun*, 40 (2014) 49-53.
- [31] A. Zadick, L. Dubau, A. Zalineeva, C. Coutanceau, M. Chatenet, When cubic nanoparticles get spherical: An Identical Location Transmission Electron Microscopy case study with Pd in alkaline media, *Electrochem Commun*, 48 (2014) 1-4.

